Simultaneous Dual-Isotope SPECT Imaging for the Detection and Characterization of Parathyroid Pathology

Donald R. Neumann

Department of Nuclear Medicine, Division of Radiology, The Cleveland Clinic Foundation, Cleveland, Ohio

A technique is described involving simultaneous, dual-isotope SPECT imaging. Using ^{123}I and ^{201}Tl, a patient study is presented, demonstrating the clinical utility of this technique in the detection and characterization of parathyroid pathology. The use of this technique in other clinical situations is discussed.

J Nucl Med 1992; 33:131–134

Various imaging methods have been used for the preoperative localization of parathyroid tumors in patients with hyperparathyroidism. Among the noninvasive methods, several scintigraphic techniques have been employed, including variations on the dual-isotope $^{201}Tl/^{99m}Tc$ subtraction techniques (*1–3*). Modification of this technique, using ^{123}I instead of [^{99m}Tc] pertechnetate, has also been proposed (*4,5*). In addition, SPECT ^{201}Tl imaging of the neck and chest in search of parathyroid pathology has also been reported (*6*).

This paper reports the use of a technique for use in the preoperative evaluation of patients with hyperparathyroidism using a dual-isotope SPECT technique for detection and characterization of abnormal parathyroid tissue.

MATERIALS AND METHODS

Following the oral administration of 300–400 μCi ^{123}I, a 6-hr radioiodine uptake is calculated, followed by the intravenous administration of 2 mCi ^{201}Tl with the patient in a resting state. After 15 min, SPECT acquisition of the neck and upper chest is performed on a dedicated, three-headed SPECT instrument (TRIAD, Trionix Research Laboratory, Inc., Twinsburg, OH). A low-energy, all-purpose, parallel-hole collimator was used on each detector. Projection data are acquired using both ^{201}Tl and ^{123}I energy windows simultaneously, maintaining data from each energy window separate. 20% energy windows were centered about the ^{123}I photopeak and the ^{201}Tl photopeak. Projection images are acquired using a 128 × 128 matrix size (pixel width = 3.56 mm). Three hundred sixty degrees of data were collected at 4-degree increments for 40 sec per projection. Total patient imaging time is approximately 20 min.

Compensation for the cross-talk contribution of each isotope into its non-primary energy window is performed on the projection data. This was done using a simple model of the imaging procedure, assuming that the counts detected in one energy window are a function of the activity of the primary isotope (n_a) and a fraction (f_b) of the non-primary isotope activity (n_b). The following equations illustrate this model:

$$N_1 = n_a + f_b n_b \qquad \text{Eq. 1}$$

and

$$N_2 = f_a n_a + n_b, \qquad \text{Eq. 2}$$

where

- N_x represents the number of counts recorded, in energy window x.
- n_a is the number of counts attributed to isotope a, having its primary photon emission associated with energy window 1.
- n_b is the number of counts attributed to isotope b, having its primary photon emission associated with energy window 2.
- f_a and f_b are the fractional contribution to the non-primary energy window attributed to isotopes a and b, respectively.

Solving for these two simultaneous equations yields:

$$n_a = \frac{N_1 - f_b N_2}{(1 - f_a f_b)} \qquad \text{Eq. 3}$$

and

$$n_b = \frac{N_2 - f_a N_1}{(1 - f_a f_b)}. \qquad \text{Eq. 4}$$

The values for $f_{I\text{-}123}$ and $f_{Tl\text{-}201}$ were determined experimentally on our instrument using both point sources and distended sources (Iowa heart phantom). Planar images on the SPECT instrument were collected using ^{201}Tl and ^{123}I separately as the isotope source in these phantoms. Once the factors $f_{I\text{-}123}$ and $f_{Tl\text{-}201}$ were determined from this data, validation of Equations 3 and 4 was then performed using planar data collected from the distended sources containing both ^{201}Tl and ^{123}I with both energy windows acquired simultaneously and placed into two separate data sets.

On our instrument, the fractional contribution from ^{201}Tl into the ^{123}I energy window was experimentally determined using phantoms of distended sources to be 0.08 ($f_{Tl\text{-}201}$), and that from ^{123}I into the ^{201}Tl energy window was 0.42 ($f_{I\text{-}123}$).

Received Mar. 7, 1991; revision accepted Jul. 19, 1991.

For reprints contact: Donald R. Neumann, MD, PhD, Department of Nuclear Medicine, Gb3, Division of Radiology, The Cleveland Clinic Foundation, Cleveland, OH 44195-5074.

Using Equations 3 and 4 on the projection data on a pixel-by-pixel basis, cross-talk compensated projection data are generated, resulting in one set of ^{201}Tl projections and one set of ^{123}I projections. A Metz filter (*7*) is applied to each cross-talk compensated projection, and tomographic reconstruction is performed using standard convolution-backprojection techniques. Two sets of transverse tomograms are produced: one representing the tomographic distribution of ^{201}Tl, and the other representing that of ^{123}I. Sixty-four 128 × 128 transverse tomograms are thus produced for each radiopharmaceutical.

Dual display of identical slices is then performed, reformatting the tomographic data into either the transverse, coronal, or sagittal plane. Once a representative slice containing normal thyroid tissue is displayed, an irregular region of interest is drawn around normal thyroid tissue on the ^{123}I tomogram. An identical region of interest is automatically mapped onto the corresponding ^{201}Tl tomogram. Total counts within these regions of interest are used for normalization of the entire set of ^{123}I tomograms, which are then subtracted from the ^{201}Tl tomographic data. This normalization/subtraction method is described by the following equation:

$$A_F(x, y, z) = A_{Tl\text{-}201}(x, y, z) - \frac{R_{Tl\text{-}201}}{R_{I\text{-}123}} \cdot A_{I\text{-}123}(x, y, z), \qquad \text{Eq. 5}$$

where $A_x(x, y, z)$ is the pixel value at coordinate (x, y, z) for either isotope x, or resultant image F, and R_x is the total number of counts within the region of interest chosen from tomographic data associated with isotope x.

The resultant tomographic images are displayed for interpretation in any of three major anatomic planes (transverse, coronal, or sagittal).

Case Report

A 62-yr-old white male, with a long history of end-state renal disease secondary to polycystic kidney disease, developed palpitations and shortness of breath. The patient had been on renal dialysis for the last 14 years. Laboratory evaluation at the time of presentation revealed hypercalcemia (11.2 mg/dl) and elevated serum parathyroid levels (1476 pg/ml) compatible with hyperparathyroidism. The patient had undergone a parathyroidectomy procedure several years previously, with surgical removal of four parathyroid glands and autotransplantation of one parathyroid gland into the left sternocleidomastoid muscle.

Simultaneous dual-isotope SPECT imaging of the neck and upper chest was performed after the oral administration of ^{123}I and intravenous administration of ^{201}Tl. Following cross-talk compensation of the projection data, SPECT reconstruction was performed followed by normalization and subtraction of the ^{123}I from the ^{201}Tl images (Figs. 1 and 2). The resultant set of SPECT images demonstrated a region of discrepant uptake of ^{201}Tl adjacent to the inferolateral aspect of the right lobe of the thyroid, measuring approximately 3.5 × 3.0 × 2.5 cm in size (Figs. 1C and 2C).

A surgical neck exploration was performed, and a parathyroid adenoma weighing approximately 8 g and measuring 3.0 × 2.0 × 1.7 cm was resected from the site identified on the SPECT study. No additional parathyroid tissue was found at the time of surgery.

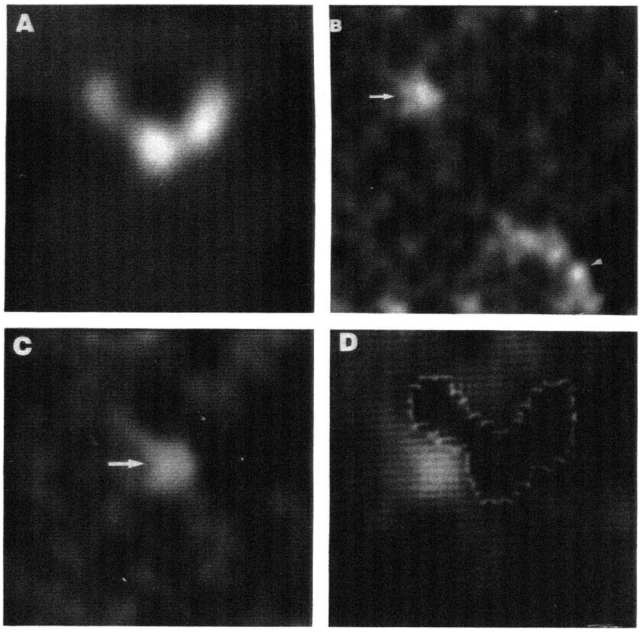

FIGURE 1. A coronal SPECT slice through the neck and upper chest of a patient with a surgically proven parathyroid adenoma. (A) Coronal ^{123}I SPECT image. Notice the distribution of the radioisotope in normally functioning thyroid tissue. (B) Coronal ^{201}Tl SPECT image. The physical location of this slice is identical to that of Figure 1A. Activity is seen associated with both the parathyroid adenoma and the adjacent thyroid (arrow). Notice the myocardial activity on this image (arrowhead). (C) Following normalization and subtraction of the SPECT ^{123}I image data in 1A from the SPECT ^{201}Tl image data in 1B, this is the resulting image. The area of discrepant ^{201}Tl accumulation (arrow) located inferolaterally to the right lobe of the thyroid corresponded to a surgically proven parathyroid adenoma. (D) Same image as Figure 1C, with the outline of the functional thyroid superimposed.

DISCUSSION

In the preoperative evaluation of patients with hyperparathyroidism, several techniques have been used in an attempt to localize abnormal parathyroid tissues (*1–5*). The dual-isotope ^{201}Tl/^{99m}Tc subtraction scintigraphic technique has been shown to be valuable for localization of parathyroid tumors in patients prior to initial surgery or in those with recurrent or persistent hyperparathyroidism after surgical neck exploration (*7–12*). Some success in identifying parathyroid adenomas has also been reported using ^{123}I/^{201}Tl subtraction scintigraphy (*4,5*). SPECT imaging using ^{201}Tl has been reported as a potentially useful technique to localize parathyroid tumors as well (*6*).

This paper describes a method for the detection and characterization of parathyroid tissue in patients with hyperparathyroidism. Because of the inherent three-dimensional characteristics of SPECT, this technique allows localization of parathyroid pathology more accurately than planar techniques. SPECT also offers the possibility to estimate lesion size in three dimensions, another advantage over planar methods (*13*). These advantages were shown in the case report, which demonstrated accurate localization of the parathyroid adenoma. The lesion size by SPECT, however, was 2.6 times the actual anatomic size.

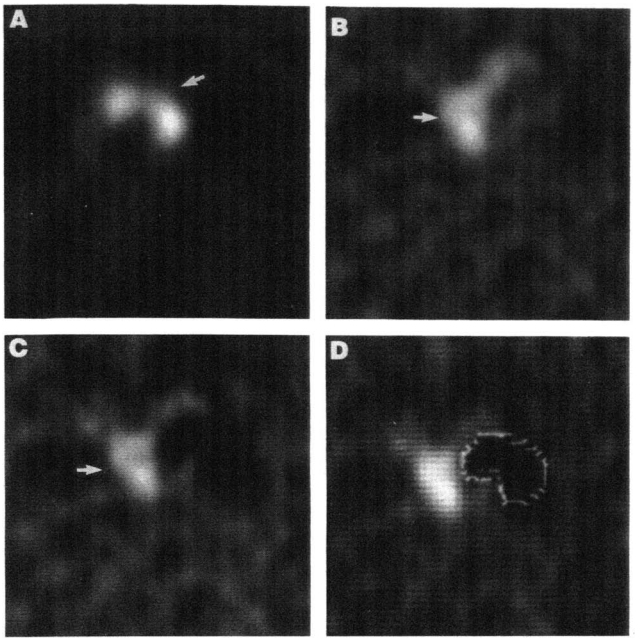

FIGURE 2. A transverse SPECT slice through the neck at the level of a surgically proven parathyroid adenoma. (A) Transverse ^{123}I SPECT image. Functional thyroid activity is seen (arrow). (B) Transverse ^{201}Tl SPECT image. The physical location of this slice is identical to that of Figure 2A. Activity within both the parathyroid adenoma and thyroid is present (arrow). (C) Following normalization and subtraction of the ^{123}I SPECT data from the ^{201}Tl SPECT data, this is a resulting transverse SPECT image, corresponding to the identical physical location as A and B. The area of ^{201}Tl accumulation (arrow) located laterally to the right lobe of the thyroid corresponded to the surgically proven parathyroid adenoma. (D) Same image as Figure C, with the outline of functional thyroid superimposed.

This over-estimation may be related to a number of factors, including the collimator used during acquisition, the spatial filter used during tomographic reconstruction, and the threshold used to define the edges of the lesion.

In conventional dual-isotope parathyroid scintigraphy, image data is collected from each of two energy windows separately (*14,15*). If the patient moves significantly between the two sets of data collection, artifacts will be introduced into the resultant normalization/subtraction images that may cause serious problems with interpretation. Alignment of the two images prior to subtraction may be difficult and if not done adequately, parathyroid lesions might be concealed or may even be artifactually created, reducing the diagnostic accuracy of this procedure. By collecting image data from both energy windows simultaneously, the problem of these types of patient motion artifacts is partially circumvented.

Should the patient move during image data collection, the effects of these motions will be introduced into both energy windows in an identical fashion. Thus, post-collection re-alignment of corresponding images is not necessary in the simultaneous, dual-isotope acquisition. Although an attempt at minimizing patient motion during image data collection should still be made, the artifacts introduced by imperfect data alignment are avoided. An additional advantage of the simultaneous dual-isotope method is the fact that total imaging time for the study is considerably reduced, improving patient tolerance for the procedure.

Because ectopic parathyroid tissue can be found in up to 20% of patients either at surgery or at autopsy (*16*), preoperative imaging of the mediastinum in addition to pinhole scintigraphy of the neck has been advocated (*17*). The field of view of the SPECT camera used in the present study allows evaluation of the neck and upper chest simultaneously.

Although this simultaneous dual-isotope SPECT technique was developed specifically for the evaluation of parathyroid pathology, the basic technique might prove useful in other clinical situations. This technique, for example, might be useful in the identification, localization and estimation of size of acute myocardial infarctions using ^{99m}Tc PYP and ^{201}Tl or ^{111}In antimyosin and ^{201}Tl (*18*). As another example, this technique might also prove useful in the evaluation of hepatic abscesses or tumors using the combination of ^{99m}Tc-sulfur colloid and ^{67}Ga-citrate.

The initial results of this technique for the localization and estimation of size of abnormal parathyroid tissue have been very encouraging. This technique is now used routinely at our institution in the preoperative evaluation of patients with hyperparathyroidism. Modifications of the technique described in this paper are presently being developed to broaden its clinical applications.

REFERENCES

1. Sandrock D, Merino MJ, Norton JA, Neumann RD. Parathyroid imaging by Tc/Tl scintigraphy. *Eur J Nucl Med* 1990;16:607–613.
2. Winzelberg GG, Hydovitz JD. Radionuclide imaging of parathyroid tumors: historical perspectives and newer techniques. *Semin Nucl Med* 1985;15:161–169.
3. Young A, Gaunt J, Croft N. Location of parathyroid adenomas thallium-201 and technetium-99m subtraction scanning. *Br Med J* 1983:286:1384–1390.
4. Picard D, D'Amour P, Carrier L, Chartrand R, Poisson R. Localization of abnormal parathyroid gland(s) using thallium-201/iodine-123 subtraction scintigraphy in patients with primary hyperparathyroidism. *Clin Nucl Med* 1987;12:60–64.
5. McKusick KA, Palmer EL, Hergenrother J. Is there a role for dual tracer imaging in detection of parathyroid disease? [Abstract]. *J Nucl Med* 1984;25:19.
6. Ziffer JA, Fajman WA. Ectopic parathyroid gland localization with thallium-201 SPECT. *Clin Nucl Med* 1987;12:617–619.
7. King MA, Doherty PW, Schwinger RB, Jacobs DA, Kidder RE, Miller TR. Fast count-dependent digital filtering of nuclear medicine images: concise communication. *J Nucl Med* 1983;24:1039–1045.
8. Manni A, Basarab RM, Plourde PV, Koivunen D, Harrison TS, Santen RJ. Thallium-technetium parathyroid scan, a useful noninvasive technique for localization of abnormal parathyroid tissue. *Arch Intern Med* 1986;146:1077–1080.
9. McFarlane SD, Hanelin LG, Taft DA, Ryan JA, Freuland PN. Localization of abnormal parathyroid glands using thallium-201. *Am J Surg* 1984;148:7–13.
10. Okerlund MD, Corpuz SW, Ling M. Parathyroid scintigraphic localization of ectopic and transplanted parathyroid glands [Abstract]. *J Nucl Med* 1986;27:963.
11. Hanty, M, Schwartz K, McClung M, Lowe DK. Technetium-thallium

scintiscanning for localization of parathyroid adenomas and hyperplasia, a reappraisal. *Am J Surg* 1987;153:479–486.
12. Kim DY, Fine EJ, Silver CE. Preoperative localization of lesions of the parathyroid gland using thallium-technetium scintiscanning. *Surg Gynecol Obstet* 1987;165:212–216.
13. Johnson LL, Lerrick KS, Coromilas J, et al. Measurement of infarct size and percentage myocardium infarcted in a dog preparation with single photon emission computed tomography, thallium-201, and indium-111 monoclonal antimyosin. Fab. *Circulation* 1987;76:181–190.
14. McCall A, Henkin R, Calandra D, Lawrence AM, Jarosz H, Paloyan E. Routine use of thallium-technetium scan prior to parathyroidectomy. *Am Surg* 1987;53:380–384.
15. Ferlin G, Borsato N, Carnerani N. New perspectives in localizing enlarged parathyroids by technetium-thallium subtraction scan. *J Nucl Med* 1983;24:438–441.
16. Rothmund M, Diethelm L, Brunner H. Diagnosis and surgical treatment of mediastinal parathyroid tumors. *Ann Surg* 1976;183:139.
17. Winzelberg GG, Hydovitz JD, O'Hara KR. Prospective comparison of Tl-201/Tc-99m pertechnetate parathyroid subtraction scintigraphy and high-resolution parathyroid ultrasonography in patients with suspected parathyroid adenomas. *Radiology* 1985;155:231–235.
18. Johnson LL, Seldin DW, Keller AM, et al. Dual-isotope thallium and indium antimyosin SPECT imaging to identify acute infarct patients at further ischemic risk. *Circulation* 1990;81:37–45.

(continued from page 126)

SELF-STUDY TEST
Gastrointestinal Nuclear Medicine
ANSWERS

a possible viral etiology. Nonbacterial gastroenteritis in humans is frequently caused by parvoviruses, such as the Norwalk and the Hawaii viruses. Histologically lesions are seen in the small intestine, but not in the stomach. Impaired gastric emptying of solids but not of liquids has been reported in these cases.

Gastric stasis has been reported with tachygastria. It has been proposed that the abnormal gastric emptying involves the local stimulation by prostaglandins, as suggested by in vitro smooth muscle depolarization studies, which have shown normalization of the frequency of pacemaker firing when indomethacin is added to the medium.

Studies of patients with psychogenic vomiting have shown that, on a clinical basis, it is very difficult to differentiate patients with idiopathic gastroparesis from those with the psychological disorder. Objective documentation of abnormal gastric motility is needed for diagnostic evaluation of such patients.

The motility of the entire gastrointestinal tract can be affected in systemic sclerosis (scleroderma). In patients with early disease, this disorder appears to affect the neuroregulatory control of the gastrointestinal tract and is manifested by incoordination of pressure activity with a decreased response of the affected part to stimulation. Evidence of gastric involvement is reported in approximately 50% of those with gastrointestinal tract involvement. Antral hypomotility is more common when there is also involvement of other areas of the gut.

Gastric stasis of solids is reported following fundoplication for hiatal hernia with reflux esophagitis. This is manifested mainly by antral hypomotility for the solid component of the meal.

References

1. Meeroff JC, Schreiber DS, Trier JS, Blacklow NR. Abnormal gastric motor function in viral gastroenteritis. *Ann Intern Med* 1980;92:370–373.
2. Peachy RD, Creamer B, Pierce JW. Sclerodermatous involvement of the stomach and the small and large bowel. *Gut* 1969;10:285–292.
3. Reed WDE, Miller LJ, Malagelada J-R. Dyspepsia, antral motor dysfunction, and gastric stasis of solids. *Gastroenterology* 1980;788:360–365.
4. Sanders K, Menguy R, Chey W, et al. One explanation for human antral tachygastria [abstr.] *Gastroenterology* 1979;76:1234.
5. You CH, Lee KY, Chey WY, Menguy R. Electrogastrographic study of patients with unexplained nausea, bloating, and vomiting. *Gastroenterology* 1980;79:311–314.

ITEMS 10–13: Gastric Emptying and the "Dumping Syndrome"

ANSWERS: 10, T; 11, T; 12, T; 13, F

When there has been resection of the distal stomach, there is decreased resistance to emptying at the large gastroenteric anastomosis. This and the decreased "receptive relaxation" of the proximal stomach secondary to vagotomy are believed to be two of the major factors in the development of the postoperative "dumping syndrome." The gastroenterostomy allows large particles to pass rapidly into the small intestine, despite decreased gastric motility. The symptoms of cramping and fullness are not primarily due to retention in the gastric pouch but rather to the rapid increase in volume in the small bowel because of the dumping of liquids and solids. The solid particles that accumulate in the small bowel are resistant to hydrolysis and can cause malabsorption and diarrhea. Some patients do develop a severe "postsurgical gastroparesis" where the proximal stomach appears unable to generate the pressure necessary to empty solids despite the large gastroenteric anastomosis.

References

1 Cheadle WG, Baker PR, Cuschieri A. Pyloric reconstruction for severe vasomotor dumping after vagotomy and pyloroplasty. *Ann Surg* 1985;202:566–572.
2 Woodward ER, Hocking MP. Postgastrectomy syndromes. *Surg Clin North Am* 1987;67:509–520.

FIGURE 1

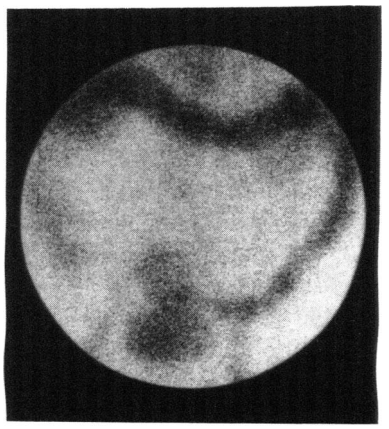

90 min

Due to a production error, the 90-min image in Figure 1 of the November 1991 Self-Study Test (p. 2063) was printed upside down. The image is pictured correctly above.

Note: For further in-depth information, please refer to the syllabus pages included at the beginning of *Nuclear Medicine Self-Study Program I: Part I.*